Multibioinspired slippery surfaces with wettable bump arrays for droplets pumping

Xiaoxuan Zhang[a], Lingyu Sun[a], Yu Wang[a], Feika Bian[a], Yuetong Wang[a], and Yuanjin Zhao[a,1]

[a]State Key Laboratory of Bioelectronics, School of Biological Science and Medical Engineering, Southeast University, 210096 Nanjing, China

Edited by David A. Weitz, Harvard University, Cambridge, MA, and approved September 9, 2019 (received for review July 19, 2019)

Droplet manipulation is playing an important role in various fields, including scientific research, industrial production, and daily life. Here, inspired by the microstructures and functions of Namib desert beetles, Nepenthes pitcher plants, and emergent aquatic plants, we present a multibioinspired slippery surface for droplet manipulation by employing combined strategies of bottom-up colloidal self-assembly, top-down photolithography, and microstructured mold replication. The resultant multilayered hierarchical wettability surface consists of hollow hydrogel bump arrays and a lubricant-infused inverse opal film as the substrate. Based on capillary force, together with slippery properties of the substrate and wettability of the bump arrays, water droplets from all directions can be attracted to the bumps and be collected through hollow channels to a reservoir. Independent of extra energy input, droplet condensation, or coalescence, these surfaces have shown ideal droplet pumping and water collection efficiency. In particular, these slippery surfaces also exhibit remarkable features including versatility, generalization, and recyclability in practical use such as small droplet collection, which make them promising candidates for a wide range of applications.

bioinspired | slippery surface | wettability | droplet | colloidal crystal

Droplet manipulation, such as droplet pumping and transportation, has attracted increasing attention in recent years for their applications in water collection, biosensing, medical analysis, chemical reactions, and so on (1–4). To realize efficient droplet manipulation, various approaches have been developed, including magnetic control, electric field guidance, reaction activation, etc. (5). Although with many breakthroughs, most of these approaches rely highly on external energy input, and could only handle droplets with specific size range, both of which place great limitations on their applications. As an alternative, functional microstructured surfaces with gradient wettability are put forward (6–12). Benefitting from their low energy input and relatively broad use range, droplet manipulation could be achieved simply and effectively based on such surfaces (13–16). However, most of these existing wettability surfaces could only handle droplets unidirectionally and carry out a single function, which are helpless in polydirectionally manipulating droplets and executing multiple tasks simultaneously. Besides, some approaches that depend on droplet growth via coalescence or condensation to provide droplet driving force seriously lower the efficiency of these surfaces in practical applications. In addition, as cleanliness determines their performance in droplet manipulation, these surfaces are hardly recyclable. Therefore, new functional wettability surface with versatile droplet manipulation ability for water collection and other applications is still sought.

In this paper, inspired by the microstructures of Namib desert beetles and Nepenthes pitcher plants, as well as pumping strategy of emergent aquatic plants, we suggest a multibioinspired surface with the desired features for droplet manipulation, as schemed in Fig. 1. Namib desert beetles could attract small water droplets from fog by using their structured backs that are composed of hydrophilic bumps and hydrophobic waxy surroundings (17); Nepenthes pitcher plants have slippery liquid-infused porous (SLIP) structured inwalls that enable them to repel liquids and induce loss-free transportation (18); while for emergent aquatic plants, they could take advantage of capillary driving force for directional pumping of objects with different sizes from a relatively long distance (19). By mimicking these remarkable creatures, many well-performed systems and devices have been designed and reported (20–23). However, due to the lack of the inspirational designs and insufficient fabrication strategies, in-depth investigations on combining multiple biological characteristics together to enhance the performance are still lacking. In addition, the practical values of these multiple biomimicked systems are seldom explored.

Herein, we combined bottom-up colloidal self-assembly (24–27), top-down photolithography (28–30), and microstructured mold replication (31) to fabricate a multilayered hierarchical wettability surface with the multibioinspired features of Namib desert beetles, Nepenthes pitcher plants, and emergent aquatic plants. This surface consisted of hollow hydrogel bump arrays and a lubricant-infused inverse opal film as the substrate. The hydrophilic bumps and hydrophobic film simulated the inhomogeneous structure of Namib desert beetles; while lubricant infusion imparted the substrate with SLIP structure like Nepenthes pitcher plants. Similar to emergent aquatic plants, the hollow hydrophilic bumps could rapidly attract and capture water droplets from all directions based on capillary driving force, which was further facilitated by the highly slippery substrate. These attracted droplets could be pumped downward through hollow channels of the bumps by capillarity and be collected by a reservoir. Notably, the droplet driving force derived only from capillary driving, rather than external energy input and droplet condensation or coalescence, bringing about ideal efficiency. It

Significance

Efficient droplet manipulation has been widely studied and used in various applications, including water treatment, chemical and biological analysis, etc. However, most of the approaches for droplet manipulation still face many challenges such as external energy dependence, single-directional droplets handling, and nonrecyclability. In this study, inspired by the features and strategies of Namib desert beetles, Nepenthes pitcher plants, and emergent aquatic plants, we present a multibioinspired slippery surface for efficient droplet manipulation by combining bottom-up colloidal self-assembly, top-down photolithography, and microstructured mold replication. It has been demonstrated that the prepared surface could well address these challenges and behave well in conducting multiplexed tasks including droplet capturing, pumping, and collecting.

Author contributions: Y.Z. designed research; X.Z. and Yu Wang performed research; X.Z., L.S., F.B., and Yuetong Wang analyzed data; and X.Z. and L.S. wrote the paper.

The authors declare no competing interest.

This article is a PNAS Direct Submission.

[1]To whom correspondence may be addressed. Email: yjzhao@seu.edu.cn.

This article contains supporting information online at www.pnas.org/lookup/suppl/doi:10.1073/pnas.1912467116/-/DCSupplemental.

First published September 30, 2019.

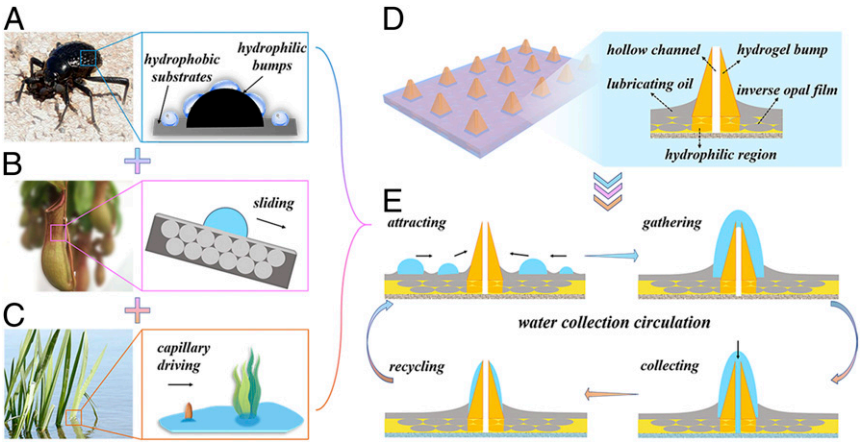

Fig. 1. Schemes of the multibioinspired slippery surfaces with wettable hollow bump arrays. (*A*) Water collection ability of Namib desert beetles, which relies on hydrophilic bumps and hydrophobic substrates on their backs. (*B*) Liquid-repelling ability of Nepenthes pitcher plants based on the SLIP structure. (*C*) Seed collecting by emergent aquatic plants, which is achieved by capillary driving. (*D*) Schematic illustrations of the structure of the surfaces. (*E*) Schematic illustrations of water pumping and collection circulation of the surfaces.

was also demonstrated that the slippery surface showed distinct versatility, generalization, and recyclability in droplet capturing, pumping, and collecting. All these results indicate that this multibioinspired slippery surface could provide an insight into droplet manipulation, and could find a variety of applications.

Results

In a typical experiment, a polyurethane (PU) inverse opal film was fabricated as the porous substrate via a sacrificial template method. During this process, the silica colloidal crystal templates were first generated by bottom-up self-assembly of SiO_2 nanoparticles on glass slides using vertical deposition. It was found that the SiO_2 nanoparticles were closely packed and formed ordered hexagonal structures after solvent evaporation (*SI Appendix*, Fig. S1). PU/Dimethyl formamide (DMF) solution was then added to the surface of the silica colloidal crystal templates, which fully filled the voids among the SiO_2 nanoparticles and got solidified upon removal of DMF. After etching the glass slide and the SiO_2 nanoparticles, the PU inverse opal film could be obtained (*SI Appendix*, Fig. S2*A*). It was worth noting that as a replication, the resultant PU film had an orderly aligned micropore structure, making it suitable to serve as the porous substrate (*SI Appendix*, Fig. S2*B*).

With the PU inverse opal film as the substrate, the slippery surface with wettable hollow bump arrays could be prepared facilely by a top-down UV mask-guided micromolding approach, as schemed in Fig. 2*A*. Specifically, a puncher was first employed to punch regularly arranged, uniform holes on the PU film (Fig. 2*B*). It should be mentioned that to ensure firm bonding between the PU film and the hollow bumps, the size of the holes was slightly smaller than the diameter of the bumps. After tidily stacking the punched film and a negative mold with ordered microcavities together, hydrogel prepolymer solution was deposited into the microcavities with a pipettor. During this process, the prepolymer solution not only filled the microcavities, but also diffused into micropores of the PU film, thus destroying the hydrophobicity of the PU film. To solve this problem and prepare hydrophilic hollow bump arrays, a specially designed mask mold that only allowed light to pass through the hollow bump array region was employed (Fig. 2*C*). In this case, when exposed to UV light, only prepolymer solution at specific regions would be cured, constructing the hydrophilic hollow bump arrays. Then by peeling off the PU film–hollow bump arrays compound from the negative mold, washing the uncured prepolymer solution away, and finally immersing the compound in

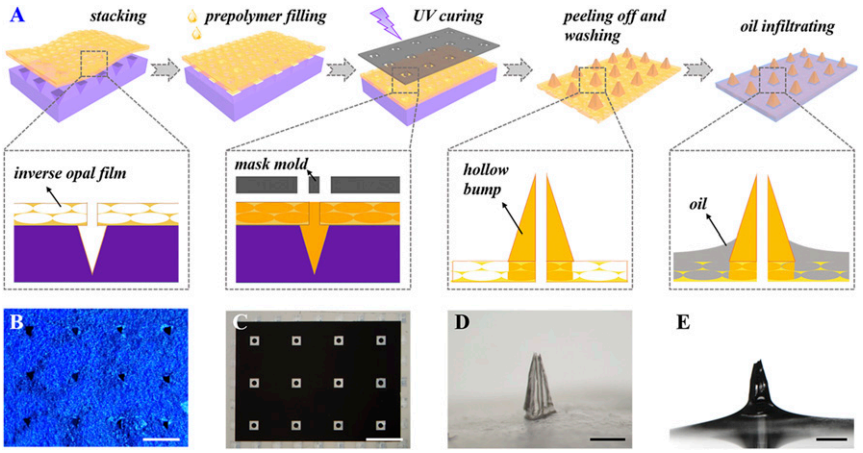

Fig. 2. Fabrication of multibioinspired slippery surfaces with wettable hollow bump arrays. (*A*) Schematic illustrations of the fabrication procedure. (*B*) Optical image of the punched PU inverse opal film. (*C*) Optical image of the tidily stacked negative mold, PU film, and mask mold. (*D*) The PU film–hollow bump arrays compound. (*E*) The lubricating oil-infused slippery surface. (Scale bars: 2.5 mm in *B* and *C*, and 550 μm in *D* and *E*, respectively.)

lubricating oil overnight, the slippery surface was achieved (Fig. 2 *D* and *E*).

Notably, the lubricating oil sufficiently infused into the micropores of PU film and covered the film surface, which mimicked the SLIP structure of Nepenthes pitcher plants and thus imparted the substrate with excellent slippery properties. These could be demonstrated by recording the water droplet sliding angle on the surface of the substrate (*SI Appendix*, Fig. S3). Results showed that the droplet was pinned to the PU film without lubricating oil infusion, because it was partly absorbed to the micropores of the film. However, the sliding angle was greatly eliminated to about 10° with the presence of lubricating oil, benefitting from the low surface energy and chemical inertia. Importantly, lubricating oil menisci surrounding the bumps were observed, which laid a foundation for droplet pumping. When a water droplet was placed onto the slippery surface, it was rapidly surrounded by lubricant menisci, as shown in *SI Appendix*, Fig. S4*A*. Because of the overlap, the lubricant meniscus between the droplet and the hollow bump was lifted up, contributing to a smaller slope angle (*SI Appendix*, Fig. S4*B*). Therefore, the horizontal component of oil/air interfacial tension pointing to the hollow bump was larger than that at the other side, generating a capillary driving force that attracted the droplet to the bump.

The capillary driving force was written as $F = \gamma R(\cos\alpha - \cos\beta)$, where γ represented oil/air interfacial tension and R represented the droplet size (19). Generally, with the increase of R, the capillary driving force increased, whereas bigger droplets also indicated larger droplet mass, bringing about lower initial acceleration and lower pumping speed (*SI Appendix*, Fig. S5*A*). It was noted that the capillary driving was considered to be applicable to all of the droplet sizes in theory, but only droplet sizes from 0.2 to 1.5 mm were tested limited to the equipment. Results showed that water droplets within that range were attracted quickly by the bump. Another factor that affected the droplet pumping was the distance from the water droplet to the bump, which could affect the angles of the oil menisci on both sides, thus having a critical influence on the capillary driving force. Generally, with the increase of the distance, the capillary driving force decreased and the driving speed reduced (*SI Appendix*, Fig. S5*B*). When the distance reached about 1.65 mm, the bump could not drive the water droplet anymore.

Taking advantage of the highly slippery substrate originated from lubricate infusion and coverage, the capillary driving force provided by lubricate meniscus, as well as the wettability of the hydrogel bumps, the prepared slippery surface exhibited excellent performance in directional droplet pumping (Fig. 3*A*). It was found that a water droplet at a distance of about 1.5 mm could be driven to the bump within 3 s, demonstrating the fast and efficient droplet pumping (Movie S1). In addition, the generalization of the slippery surface was investigated by changing the materials of the bump and types of the lubricating oil, observing the pumping phenomenon, and recording the droplet pumping time (Fig. 3 *B* and *C*). It could be seen that the bumping efficiency remained almost unchanged when the bump material was varied from poly(ethylene glycol) diacrylate (PEGDA) to trimethylolpropane ethoxylate triacrylate (ETPTA) or the lubricating oil was varied from silicone oil to perfluorinated oil. We also evaluated the effect of stiffness and composition of the hydrogel bump by altering the concentration of PEGDA or mixing PEGDA with polyacrylamide (AAm). Results showed that the bumping time stayed at about 2.5 s upon first use, which was relatively insensitive to the hydrogel stiffness and composition (*SI Appendix*, Fig. S6). All of these indicated that this pumping strategy was versatile and dynamic. It should be mentioned that for the bumps containing over 25% PEGDA, they would deform slightly when contacting large water droplets. After the droplets completely enveloped the bumps, the bumps would restore to the original state, making no difference to their continuous operations. However, for the 10% AAm bumps, which were too soft and swellable, the deformation was irreversible, which inevitably affected the continuous use.

The attracted droplets soon gathered around the hollow bump, enveloped the bump, and infiltrated downward through the hollow channel by capillarity until being completely absorbed by a porous support (*SI Appendix*, Fig. S7). Therefore, via this droplet attracting, water gathering, and collecting circle, droplets could be successfully collected, as shown in Movie S2. The droplet with the diameter of 1 mm at a distance of 1.5 mm was pumped and collected within 10 s. Also, the amount of residual liquid was relatively small, thus not significantly changing the oil meniscus and water transport/collection efficiency. Besides, the slippery surface could sequentially pump and collect droplets, which was briefly confirmed by the collection of 3 consecutive water droplets in *SI Appendix*, Fig. S8. Apart from the continuous droplet pumping and collection, pumping and collecting of droplets from different directions could also be achieved. To prove it, water droplets were added to the same slippery surface from 4 different directions—the top right, the top left, the bottom left, and the bottom right, respectively. During this process, all droplets were found to be pumped to the hollow bump and collected (Fig. 4 *A*–*D*). All these features enabled the slippery surface to be beneficial to water collection in practice.

To explore their practical value in water collection, these slippery surfaces were sprayed with microdroplets generated by a sprayer. After being rapidly encircled by lubricating oil menisci, most of these microdroplets, regardless of the size, quickly gathered at the

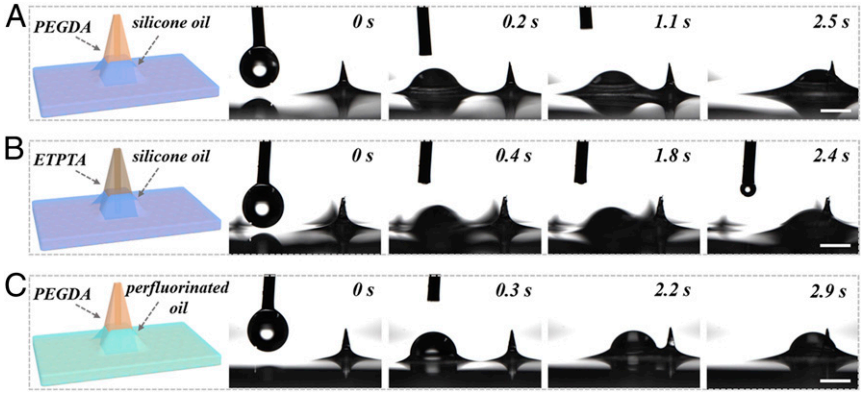

Fig. 3. Schemes and optical images of directional droplet pumping by the slippery surface. (*A*) PEGDA as the bump material and silicone oil as the lubricant; (*B*) ETPTA as the bump material and silicone as the lubricant; (*C*) PEGDA as the bump material and perfluorinated oil. (All scales bars: 750 μm.)

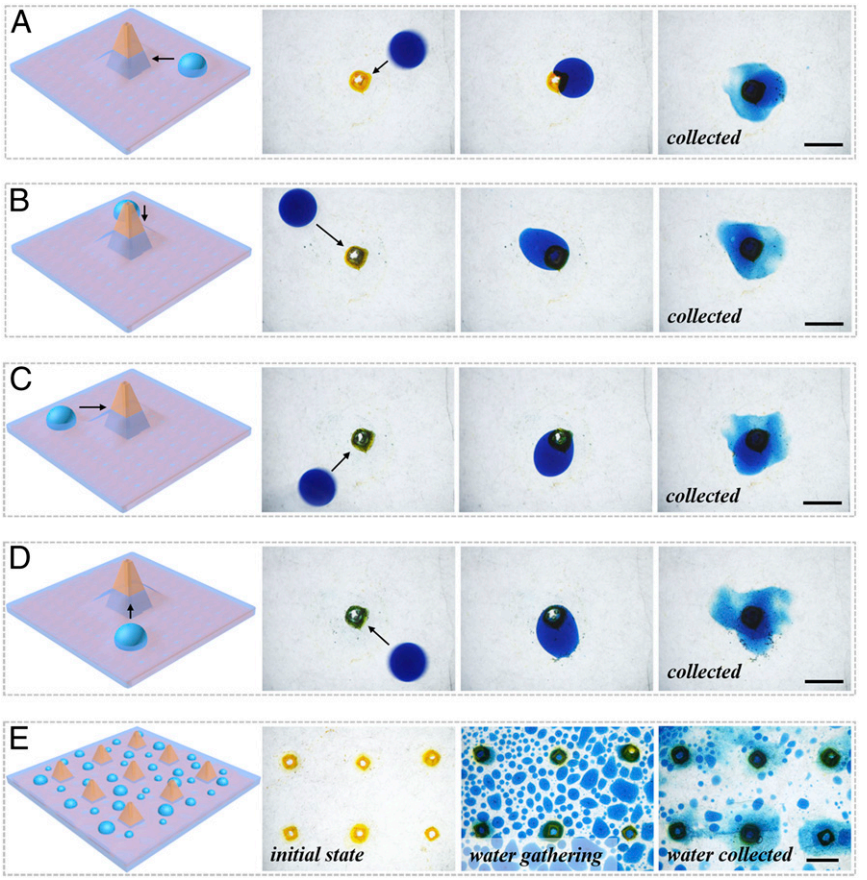

Fig. 4. Schemes and optical images of water collection by the slippery surface. (*A–D*) Pumping and collection of droplets from different directions; (*E*) pumping and collection of a large number of sprayed microdroplets. (All scale bars: 1 mm.)

nearby bump (Movie S3). It was noteworthy that during this process, some microdroplets first converged into a bigger one before being transported to their destination. Finally, except a small amount, majority of the microdroplets were collected, indicating the relatively ideal behavior of the slippery surfaces in sprayed water collection (Fig. 4*E*). These unstable residual water droplets did not affect the lubricant menisci around the bumps significantly and were likely to be collected by the bumps after contact with new water droplets in the next round of water collecting. Strikingly, there was no extra energy input in the whole collection course. Also, the directional droplet pumping only depended on capillary driving force provided by lubricant menisci, without the need of droplet condensation or coalescence. These remarkable properties demonstrated that these slippery surfaces were effective.

Based on the desired functions of the slippery surfaces, a water collector constituted by such slippery surface, a porous support, and a reservoir was devised and set up (Fig. 5*A*). The operational procedure of this collector was pretty simple, during which the sprayed water droplets were first collected by the slippery surface, then absorbed by the porous support, and eventually flew down along the wall of the reservoir to be accumulated. Parameters that would have impacts on the water collection efficiency, such as the diameter of the hollow channels, the spacing between the adjacent bumps, and the height of the bumps, were further studied (*SI Appendix*, Fig. S9). Specifically, when the hollow channel widened, the water collection velocity would increase correspondingly, probably because the narrow channel restricted the infiltration of gathered droplets; while this ascending trend gradually slowed down and even ceased as the diameter reached about 350 μm (Fig. 5*B*). In addition, reduced bump spacing would result in improved water collection velocity, since the decrease of distance between droplets and bumps was typically followed by the increase of capillary driving force (Fig. 5*C*). However, when the spacing was as near as 2 mm, the water collection velocity was no longer affected by the spacing. Similarly, with the descending of the bump height, the water collection velocity rose up and finally plateaued (Fig. 5*D*). This increase could be explained by the more attracted droplets required to envelop higher bumps and realize infiltration compared to shorter bumps. Specially, after the collecting process was completed, all of the collectors could collect more than 70% of the water sprayed to the collector (*SI Appendix*, Fig. S10). For the optimal situation, the proportion was about 91%.

Note that the water collector showed satisfactory results in recyclability test (*SI Appendix*, Figs. S11 and S12). In this test, water droplets were first sprayed to the water collector. After the collector had completely collected the droplets, the reservoir was detached, weighed, and put back to its original place again. This water spraying–droplet collecting–reservoir weighing cycle was first carried out 10 times in succession. On the basis of the weight change, water collection efficiency for each circle was calculated. It could be seen that with the increase of cycles, the water collection efficiency remained constant and the collector itself kept stable and integral. To further show the collector's resiliency and consistency, this cycle was then repeated 150 times and the water collection efficiency for every 15 cycles was recorded using the same method. Results showed that during the 150 cycles, the collector could well retain its water collection efficiency. Therefore, the water collector was demonstrated to perform well in

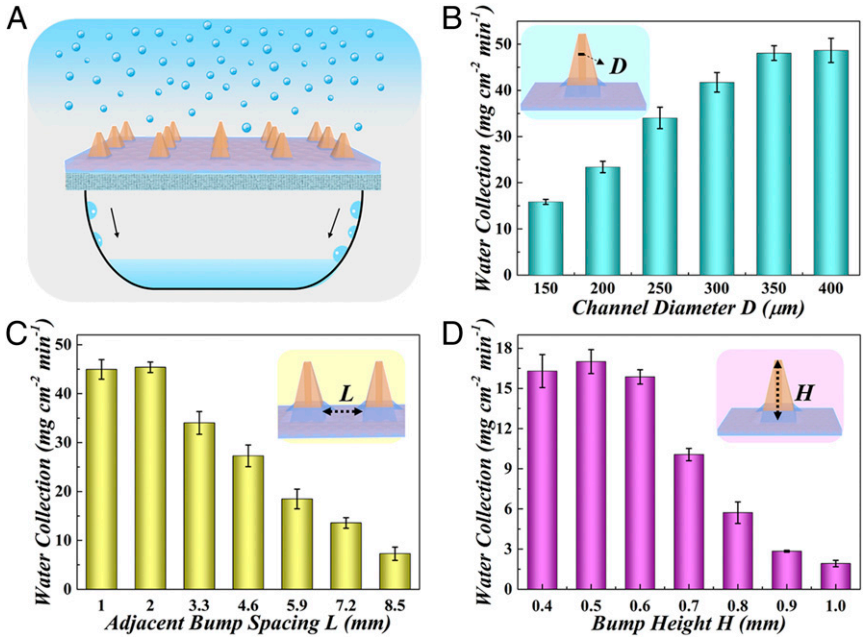

Fig. 5. Water collection performance of the slippery surface device. (*A*) Schematic illustration of the slippery surface device. (*B–D*) Water collection efficiency as function of channel diameter (*B*), adjacent bump spacing (*C*), and bump height (*D*).

repeatable utilization, indicating that it would provide an effective approach in water collection field.

Discussion

In summary, we have presented multibioinspired slippery surfaces with wettable hollow bump arrays for directional water droplet pumping and collection, which were fabricated by combined approaches of bottom-up colloidal self-assembly, top-down photolithography, and microstructured mold replication. Mimicking the structured backs of Namib desert beetles, the SLIP inwall of Nepenthes pitcher plants, as well as the capillary driving force of emergent aquatic plants, these surfaces were demonstrated to realize continuous, multidirectional water droplet attracting and pumping. The attracted droplets then gathered around the bump arrays, infiltrated downward through hollow channels of the bumps by capillarity, and finally got collected by a reservoir. Because the pumping was independent of applied energy, droplet condensation, or droplet coalescence, these surfaces showed ideal efficiency. Moreover, these surfaces were highly versatile and easy to be generalized, as they could retain their high efficiency when materials of bumps and other parameters were changed. Their recyclability was also demonstrated via a repeated water collection test. Benefitting from these distinctive features, the slippery surfaces could open a promising avenue to water transportation and droplet collection.

In nature, many organisms have evolved special structures and strategies to adapt to the environment and survive. Introduction of these marvelous structures and strategies into droplet manipulation systems is an ingenious idea, about which numerous researches have been carried out (32–36). Despite their remarkable advantages, many of these systems only simulated a single or some functionally similar biological structures, leading to a relatively simple function and an inflexible operation. Compared to previous devices, we present a principle and method that combined droplet pumping and droplet collection together. Our slippery surfaces mimic the structures of Namib desert beetles and Nepenthes pitcher plants, as well as the pumping strategy of emergent aquatic plants, and possess desired features for droplet manipulation. In addition to droplet collection, these slippery surfaces are also potential to act as microreactors and arouse inspirations in biomedical analysis, analytical chemistry, etc. To implement these values, future endeavors will be focused on improving their vapor condensation ability and realizing integration with other platforms.

Materials and Methods

Materials. SiO_2 nanoparticles were self-prepared in the laboratory. PU (average Mw is about 16,800) was acquired from Mackun. DMF was bought from Aladdin. PEGDA (average Mw is about 700) and ETPTA (average Mw is about 912) were obtained from Sigma-Aldrich. Silicone oil (50 CS) was purchased from Shin-Etsu Chemical Co., Ltd. Perfluorinated oil was provided by DuPont. Deionized water with a resistivity of 18.2 $M\Omega \cdot cm^{-1}$ was purified by a Milli-Q Plus 185 water purification system (Millipore). All reagents were of analytical grade and used as received.

Characterization. Droplet pumping, water infiltration, and sliding angles were characterized using a JC2000D2 contact angle measuring system. Bumps with different hollow channel diameters were observed under a Laser Scanning Confocal Microscope (Carl Zeiss, LSM510). Other optical images and videos were taken by a stereomicroscope (Olympus BX51) equipped with CCD (AOS Technologies AG). Scanning electron microscope (SEM) images were obtained from a Hitachi S-3000N SEM.

Fabrication of the PU Inverse Opal Film. The PU inverse opal film was fabricated by sacrificing silica colloidal crystal templates. The silica colloidal crystal templates were prepared by first assembling SiO_2 nanoparticle solution on glass slides by a vertical deposition method and then evaporated the solvent. After that, PU/DMF solution (20% wt/vol) was added dropwise to the templates and infused into the voids among SiO_2 nanoparticles. After heating at 75 °C for 1 h to fully get rid of DMF solvent, the composite film was immersed in hydrofluoric acid (HF) solution (4% vol/vol) overnight. By finally washing away HF, the PU inverse opal film was obtained.

Fabrication of the Slippery Surface. Uniform, orderly arrayed holes were first made through the PU inverse opal film with a puncher. The punched film was then tidily stacked with a negative mold with ordered microcavities. Using a pipettor, PEGDA prepolymer solution (50% vol/vol) was deposited to the negative mold, which diffused into both the microcavities and the micropores of the PU inverse opal film. With a UV mask to block light at specific regions, PEGDA hollow bump arrays bonded to the PU inverse opal film could be fabricated by UV solidification. In addition, PEGDA prepolymer solution that diffused into the micropores of the film under the bump regions was also solidified, forming a composite of the inverse opal scaffold and PEGDA

hydrogel around the hollow channel, which was entirely hydrophilic. The compound was gently stripped out from the negative mold, ultrasonic cleaned in ethanol 3 times, and immersed in lubricant oil overnight. Thus, the slippery surface with wettable bump arrays was prepared. Notably, by choosing high concentration of highly cross-linked PEGDA as the material of the bump array, the volume of the bumps would not change evidently during hydrogel swelling, thus guaranteeing their stability.

Water Collector Setup. The water collector was composed of the slippery surface, a porous support (e.g., sponge), and a reservoir. The slippery surface was for droplet collection. The porous support served to prop up the soft slippery surface as well as assist absorbing and guiding water. And, the reservoir could hold the collected water.

Measurement of Water Collection Efficiency. A facial sprayer (flow velocity at 60–75 mL h^{-1}, Shenzhen Jisu Technology Co., Ltd) was employed to generate microsized water droplets. The distance between the slippery surface and the sprayer was fixed at 1.5 dm. The total quantity of water provided to the environment was 1–1.25 g and the water that fell onto the slippery surface was about 0.92 g. After the water collection was finished, the reservoir was weighed. The water collection efficiency was then calculated based on the weight change, which was as follows:

$$water\ collection\ efficiency = \frac{w_t - w_0}{S_{surface}} \Big/ t_{collection}, \quad [1]$$

where w_t was the weight of the reservoir after collection, w_0 was the weight of the reservoir before collection, $S_{surface}$ was the superficial area of the slippery surface, and $t_{collection}$ was the total collection time. Notably, as the hollow bumps were in the microscale and the collector was tested and generally used in the humid environment, the water volume sprayed did not affect the water collection efficiency.

ACKNOWLEDGMENTS. This work was supported by the National Key Research and Development Program of China (2017YFA0700404), the National Natural Science Foundation of China (NSAF) (Grant U1530260), the Natural Science Foundation of Jiangsu (Grant BE2018707), and the Scientific Research Foundation of Southeast University.

1. Z. Huang *et al*., A general approach for fluid patterning and application in fabricating microdevices. *Adv. Mater.* **30**, e1802172 (2018).
2. H. Wang *et al*., Biomimetic enzymes cascade reaction system in microfluidic electrospray microcapsules. *Sci. Adv.* **4**, eaat2816 (2018).
3. H. Kim *et al*., Water harvesting from air with metal-organic frameworks powered by natural sunlight. *Science* **356**, 430–434 (2017).
4. T. Mouterde, P. S. Raux, C. Clanet, D. Quéré, Superhydrophobic frictions. *Proc. Natl. Acad. Sci. U.S.A.* **116**, 8220–8223 (2019).
5. L. Shang, Y. Cheng, Y. Zhao, Emerging droplet microfluidics. *Chem. Rev.* **117**, 7964–8040 (2017).
6. T. Wang, Y. F. Si, S. Q. Luo, Z. C. Dong, L. Jiang, Wettability manipulation of overflow behavior via vesicle surfactant for water-proof surface cleaning. *Mater. Horiz.* **6**, 294–301 (2019).
7. J. Wang *et al*., Bioinspired shape-memory graphene film with tunable wettability. *Sci. Adv.* **3**, e1700004 (2017).
8. H. Li *et al*., Spontaneous droplets gyrating via asymmetric self-splitting on heterogeneous surfaces. *Nat. Commun.* **10**, 950 (2019).
9. J. Li *et al*., Directional transport of high-temperature Janus droplets mediated by structural topography. *Nat. Phys.* **12**, 606–612 (2016).
10. J. Kim *et al*., Nonlinear frameworks for reversible and pluripotent wetting on topographic surfaces. *Adv. Mater.* **29**, 1605078 (2017).
11. X. He *et al*., Synthetic homeostatic materials with chemo-mechano-chemical self-regulation. *Nature* **487**, 214–218 (2012).
12. G. Trujillo-de Santiago *et al*., Chaotic printing: Using chaos to fabricate densely packed micro- and nanostructures at high resolution and speed. *Mater. Horiz.* **5**, 813–822 (2018).
13. J. Wang *et al*., Programmable wettability on photo-controlled graphene film. *Sci. Adv.* **4**, eaat7392 (2018).
14. S. N. Zhang, J. Y. Huang, Z. Chen, S. Yang, Y. K. Lai, Liquid mobility on superwettable surfaces for applications in energy and the environment. *J. Mater. Chem. A* **7**, 38–63 (2019).
15. J. Choi *et al*., Flexible and robust superomniphobic surfaces created by localized photofluidization of azopolymer pillars. *ACS Nano* **11**, 7821–7828 (2017).
16. D. Chen, G. H. McKinley, R. E. Cohen, Spontaneous wettability patterning via creasing instability. *Proc. Natl. Acad. Sci. U.S.A.* **113**, 8087–8092 (2016).
17. K. C. Park *et al*., Condensation on slippery asymmetric bumps. *Nature* **531**, 78–82 (2016).
18. T. S. Wong *et al*., Bioinspired self-repairing slippery surfaces with pressure-stable omniphobicity. *Nature* **477**, 443–447 (2011).
19. J. Jiang *et al*., Directional pumping of water and oil microdroplets on slippery surface. *Proc. Natl. Acad. Sci. U.S.A.* **116**, 2482–2487 (2019).
20. H. Chen *et al*., Continuous directional water transport on the peristome surface of Nepenthes alata. *Nature* **532**, 85–89 (2016).
21. Z. Dong *et al*., Superoleophobic slippery lubricant-infused surfaces: Combining two extremes in the same surface. *Adv. Mater.* **30**, e1803890 (2018).
22. R. J. Hu *et al*. A bioinspired hybrid membrane with wettability and topology anisotropy for highly efficient fog collection. *J. Mater. Chem. A* **7**, 124–132 (2019).
23. S. Amini *et al*., Preventing mussel adhesion using lubricant-infused materials. *Science* **357**, 668–673 (2017).
24. C. H. Liu *et al*., Tunable structural color surfaces with visually self-reporting wettability. *Adv. Funct. Mater.* **26**, 7937–7942 (2016).
25. M. Wang, Y. Yin, Magnetically responsive nanostructures with tunable optical properties. *J. Am. Chem. Soc.* **138**, 6315–6323 (2016).
26. F. F. Fu, L. R. Shang, Z. Y. Chen, Y. R. Yu, Y. J. Zhao, Bioinspired living structural color hydrogels. *Sci. Robot.* **3**, eaar8580 (2018).
27. Z. Li, Y. Yin, Stimuli-responsive optical nanomaterials. *Adv. Mater.* **31**, e1807061 (2019).
28. G. H. Lee *et al*., Chameleon-inspired mechanochromic photonic films composed of non-close-packed colloidal arrays. *ACS Nano* **11**, 11350–11357 (2017).
29. Y. S. Zhang, A. Khademhosseini, Advances in engineering hydrogels. *Science* **356**, eaaf3627 (2017).
30. M. Sun *et al*., Hydrogel interferometry for ultrasensitive and highly selective chemical detection. *Adv. Mater.* **30**, e1804916 (2018).
31. F. Fu *et al*., Bio-inspired self-healing structural color hydrogel. *Proc. Natl. Acad. Sci. U.S.A.* **114**, 5900–5905 (2017).
32. H. Bai *et al*., Efficient water collection on integrative bioinspired surfaces with star-shaped wettability patterns. *Adv. Mater.* **26**, 5025–5030 (2014).
33. S. Zhang, J. Huang, Z. Chen, Y. Lai, Bioinspired special wettability surfaces: From fundamental research to water harvesting applications. *Small* **13**, 1602992 (2017).
34. C. Li *et al*., Fog harvesting of a bioinspired nanocone-decorated 3D fiber network. *ACS Appl. Mater. Interfaces* **11**, 4507–4513 (2019).
35. H. Chen *et al*., Ultrafast water harvesting and transport in hierarchical microchannels. *Nat. Mater.* **17**, 935–942 (2018).
36. J. Lin, X. Tan, T. Shi, Z. Tang, G. Liao, Leaf vein-inspired hierarchical wedge-shaped tracks on flexible substrate for enhanced directional water collection. *ACS Appl. Mater. Interfaces* **10**, 44815–44824 (2018).